HardwareX 14 (2023) e00437

Contents lists available at ScienceDirect

HardwareX

journal homepage: www.elsevier.com/locate/ohx

Hardware Article

Kinetic adhesion test to determine particle surface energy

Lorenzo Pedrolli [a,b], Sadegh Nadimi [a,*], Sadaf Maramizonouz [a], Beatriz Achiaga Menor [b], Alejandro López [b]

[a] School of Engineering, Newcastle University, UK
[b] Applied Mechanics, University of Deusto, Spain

ARTICLE INFO

Article history:

Keywords:
Adhesion
Contact mechanics
Particles
Surface energy
Impact

ABSTRACT

A new hardware is described to quantify the particle surface energy by assuming that the Johnson Kendall and Roberts theory of elastic-adhesive contacts is applicable. The setup is used in the active section of the measurement, where newly designed elements provide the sharp impact needed to detach the particles under the action of their own kinetic energy. It employs a selection of sensors to provide the necessary measurements in a streamlined procedure, which lets the user complete one test in less than one minute. The temporal resolution is 1 µs for the contact time measurement and the velocity has a repeatability of 1%. The surface energy is a significant parameter for the characterisation of particulate materials and is widely used in Discrete Element simulations of the bulk behaviour.

1. Specifications table

Hardware name	Kinetic Adhesion Test
Subject area	Engineering and material science
Hardware type	Measuring physical properties and in-lab sensors
Closest commercial analog	No commercial analog is available
Open source license	CC BY 4.0
Cost of hardware	€1300
Source file repository	https://doi.org/10.5281/zenodo.7448231; Editable CAD design files are available as an Onshape public repository here.

* Corresponding author.
E-mail address: sadegh.nadimi-shahraki@ncl.ac.uk (S. Nadimi).

https://doi.org/10.1016/j.ohx.2023.e00437
2468-0672/

2. Hardware in context

Fine particulate materials can be characterised by various levels of adhesion or stickiness. This characteristic affects their physical, mechanical, chemical and hydraulic behaviour and is significant in a range of applications from pharmaceutical processing to powder-based additive manufacturing [1]. Van der Waals forces (F_{vdw}) are dominant in fine particles, followed by electrostatic forces in the presence of high charges (F_{es}), and capillary forces at high humidity levels (F_c). Johnson, Kendall and Roberts (JKR) proposed one of the widely adopted elastic-adhesive contact models [2]3. In this model, a spherical particle in contact with a surface, under no external loads, produces a finite contact radius a as described by Hertz theory [4] for the contact of perfectly elastic spheres due to the attractive forces. The energy in the system at any time includes stored elastic strain energy U_E and the surface energy $U_S = -\pi a^2 \Gamma$, where Γ is the energy per unit contact area.

There exists a few methods to determine the adhesive forces in the microscale. Atomic Force Microscopy (AFM) allows for a direct measurement of the force–displacement curve, for micron sized particles on atomically flat surfaces [5]. The obtained measurements are heavily influenced by the local curvature and asperities, resulting in values that are lower than what can be expected by the JKR theory. A single contact can be evaluated at any time, therefore several measurements are needed to characterize even a single particle, resulting in unpractical long measurement times for engineering applications. To similarly determine the adhesive properties of a single particle, Shukla and Henthorn [6] use a microfluidic channel to determine the fluid velocity needed to detach a particle from the channel wall. Hoshino et.al. [7] use an electrostatic detachment method to determine the adhesion force of charged toner particles. This method is suitable only for charged particles.

To assess the bulk properties of powder flow, commonly used methods rely on proxies that represent the process conditions as closely as possible. The experimental results obtained by such test devices are then used to calibrate the contact model parameters by matching the proxy to its simulation. Several device exist which are capable to apply a variety of loads to determine the bulk density, cohesion, internal and wall angles of friction, unconfined yield stress and tensile failure stress to name a few [8]. The parameters determined with these technique are useful in simulating the behavior in cases similar to the proxy itself, but generally lack generalization since the technique infers the microscale parameters rather than directly measuring them.

In the centrifugal method particles are placed on a rotor that realizes a rotating frame, with the adhesion between particle and substrate providing the centripetal force needed to sustain the rotational motion. PSD analysis before and after centrifugation is used to determine the adhesive parameter Γ [9] [10]. The quasi-static fore applied to the particles tends to approximate the thermodynamic work of adhesion W, but it may leave out an important dependency of the crack propagation speed on the adhesive energy Γ [11].

The objective of this work is to provide a device which is capable to bridge the gap between the bulk scale and micro-scale characterization of the adhesive characteristics of powders, allowing the direct measurement of the micro-scale surface energy on a large sample at the same time. The proposed hardware conceptualised from the JKR theory in which the particles attracted on a surface of interest will be subjected to an impact force and if they are large enough they will detach from the surface. By quantifying the particle size distribution (PSD) before and after the impact, determining the critical size above which the inertia is sufficient to detach the particle and measuring the impact velocity and contact time, the parameter Γ can be quantified. This consideration extends to other cohesive contact models, namely: Bradley, DMT, Maugis-Dugdale or the aforementioned JKR. The user can adapt the post-processing step to the more appropriate formulation for the case under examination.

As opposed to the complementary centrifuge method, the objective is to apply the load as an impulse, therefore obtaining an adhesive energy that could be better suited to describe the impacts between particles, for instance during the pneumatic conveying in dilute phase.

In the previous implementation reported in [12], the setup consisted of a vertical transparent tube, serving as a guide to the falling sample, and an annular stopper at the bottom. The velocity and contact time of the falling sample were both recorded by a high-speed camera; the article reports a speed of 75000 frames per second, therefore a time resolution of 13.3μs. Both the velocity measurement and the contact time estimation require a post-processing step on the video recording of the test. The new setup enhances the measurement by using electronic sensors, magnetic control of the sample, isolating the response of the stopper, and new formulations that minimise the post-processing.

3. Hardware description

The presented device aims to provide a reliable platform to conduct particle's adhesion test through kinetic impacts. It consists of a sample carrier which falls on an anvil. The carrier is magnetically held in place until the moment of release.

The micro-controller unit monitors the fall through a precise timing of the release, the passage through a photoelectric switch beam, and the moment of impact, as well as handling the communication with the operator and handling the sequence of events of the test. The sensors are active only during the test, and deactivated otherwise. The IONO MKR platform has been chosen to support the 24V sensors and provide a layer of protection to the Arduino MKR WiFi 1010 board, which has been chosen to provide Bluetooth Low Energy (BLE) connectivity.

The aluminium frame is built using OpenBuilds extrusions and carriage. The anvil height adjustment and the photoelectric switch are held by 3D-printed parts. The wiring is held in a 3D printed enclosure with a laser-cut lid.

The device can be used to:

- Characterise particles' surface energy
- Sharp impact testing of a sample
- Adapt to strain-rate dependent tests

3.1. Anvil

The anvil's mass and surface hardness are responsible for the dynamic of the impact. The impact is suspended on three springs to isolate its response from the surrounding elements: the structure and the bench. The top surface is ground flat and ideally is hardened. The bottom presents three flat-bottom holes for the spring sleeves and six mounting holes for the sensors.

The objective is to approximate a two-bodies elastic collision, where one body is reasonably larger than the other. In this hardware, the anvil size has been chosen to be approximately 10 times the mass of the impacting carrier and sample. Given a mass of 2.7kg, or a weight of 26.6N, the anvil is suspended on three springs with an elastic constant of $0.7N/mm$ each. The total compression at rest is then 12.7mm, and the characteristic frequency f_c is much lower than the expected impact dynamic, providing isolation between the impact and the ground:

$$f_c = \frac{\omega}{2\pi} = \frac{1}{2\pi}\sqrt{\frac{k}{m}} = 27.8\text{Hz} \quad (1)$$

The spring sleeves and adjustment screws can be easily modified to accommodate springs of different stiffness. The adjustment screws (#220–002) are held by three respective 3D-printed brackets, fixed on the base of the frame by screws and T-nuts.

One normally closed vibration switch is present under the anvil. As the anvil is disturbed, it activates and sends an interrupt signal to the microcontroller, which records the impact instantly. This value will be used in addition to the photoelectric switches activation times to determine the impact velocity. Compared to the direct measurement of the touch between the carrier and anvil there is a 66μs delay (measured through a 100MHz oscilloscope), attributable to the elastic wave propagation, retarded motion of the anvil, and the response time of the switch.

By placing the three switches in a triangular pattern it should be possible to detect impacts happening in a non-flat orientation. In such a configuration, a comparator would trigger the interrupt, then an analog reading could be used to determine which and how many switches activated. The schematic provided in Fig. 2 suggests a simple resistor network to perform that. If all the resistors have the same value (10kΩ), it is possible to know how many are activated. If the supply is 24V, the voltage readings are resumed in Table 1. In the final version, this technique has not been implemented due to the higher complication of the switch circuitry, and the need of a reliable interrupt signal conflicting with an analog value read.

A piezoelectric accelerometer can be used to record the anvil acceleration upon impact, a_{anvil}. It is advisable to consider it as an option. Using Newton's second and third laws of motion, the mass ratio between anvil and carrier can be used to determine the acceleration of the carrier, and therefore of the particles that are able to remain in contact with the test surface:

$$a_{carrier} = a_{anvil}\frac{m_{anvil}}{m_{carrier}} \quad (2)$$

The carrier deceleration value can be used to determine the surface energy per unit area:

$$a_{carrier} = \frac{3}{2}\pi R_c \Gamma \frac{1}{m_c} \quad (3)$$

where R_c and m_c are respectively the critical radius and mass from the sample powder. The highest value reported in [12] is $44.6 \times 10^3 \text{m/s}^2$, or 4542g. Considering Eq. 2, the accelerometer should be able to read at least 500g. A starting point is the low-cost embeddable accelerometer model 66102APZ1 by Amphenol PCB Piezotronics, or the equivalent 805–0500 by TE Connectivity. Both of these products use a two-wire read configuration, which requires a current setting diode, to provide a constant current of $2 - 20$mA. From the TE Connectivity datasheet, the suggested circuit is reported in Fig. 3. The blocking capacitor C1 realizes an AC coupling to the recording circuit, but it is needed to pre-condition the signal against slow drift. A simple resistor network can be used to shift the signal back to the center of the ADC sensing range. It must be noted that the accelerometer signal can go as high as the supply voltage (24V), therefore it must be carefully conditioned before being passed to the microcontroller. The board selected for this application (IONO MKR) allows for voltage readings with the range $0 - 30$V.

3.2. Carrier

The carrier, made of ferromagnetic steel, can be attached to the top magnet, from which it is dropped to the anvil. Ideally, the impacting surface is hardened. In this design, the carrier presents a cavity for sample stubs of $\varnothing 30 \times 10$mm, with one of

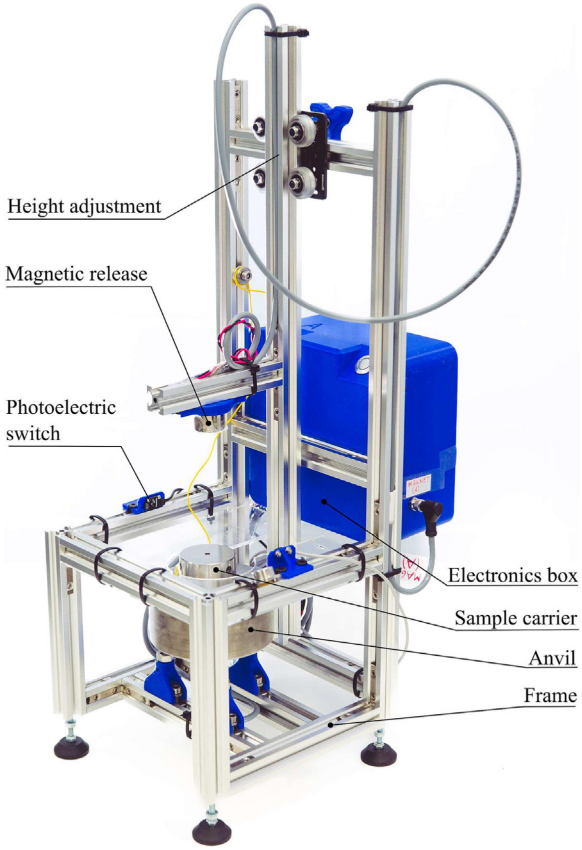

Fig. 1. Annotated view of the device.

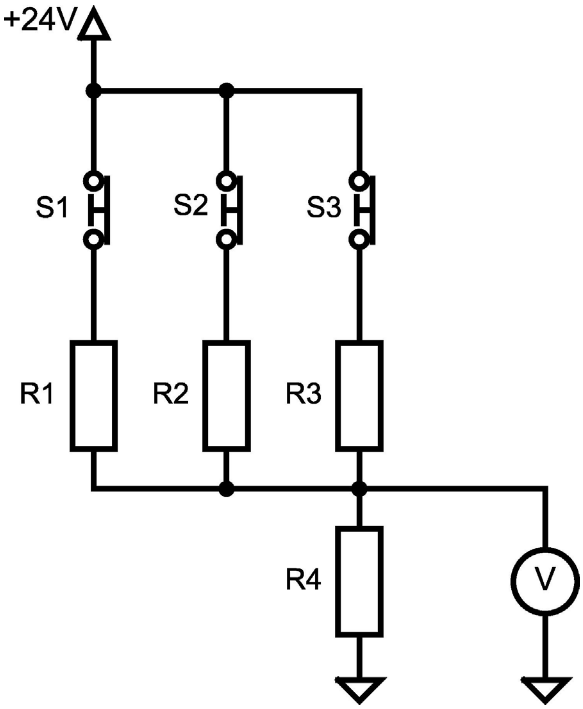

Fig. 2. Circuit to detect multiple switches activation using one analog pin.

Table 1
Analog values to determine number of closed switches.

Number of closed switches	measured voltage
3	18
2	16
1	12
0	0

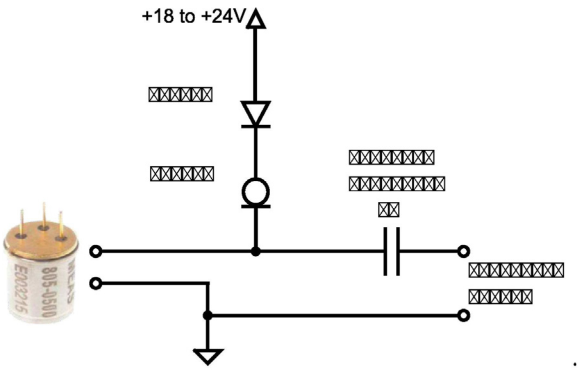

Fig. 3. Accelerometer 2-wire circuit suggested by TE Connectivity.

the circular surfaces holding the powder particles. A hole on the back of the carrier can be used to insert either a screw or a stick to aid in lowering and raising the sample. Once it is placed, three setscrews hold the sample in place. Once the sample has been loaded, the mass should be recorded for Eq. 2. The presented design suggests the use of monolithic sample stubs, where the substrate is the top surface in Fig. 4. This is possible for commonly available materials, but a thin substrate can be securely adhered to the surface, for instance using cyanoacrilate adhesive or any appropriate bonding method. The stub can also be molded in resin, containing samples which might be used for metallographic analysis at any point before or after this test: the 30mm diameter was motivated by this use case.

The carrier has a wire that connects it to the micro-controller. This has been added to precisely record the contact duration between the carrier and the anvil. Inside the IONO MKR unit, the digital inputs have a pulldown resistor, therefore the carrier is at ground potential. The anvil is connected to the supply voltage (24V) through a 10kΩ resistor. The voltage is applied only during the testing phase, when the operator should not touch the device. At the moment of impact the circuit is closed, and the signal goes high. As the carrier rebounds and leaves the anvil, the circuit opens again and the signal is pulled down to ground. The typical contact time during the impact has been measured using a 100MHz oscilloscope to be in the order of 50 to 200μs. The micro-controller is able to record the contact time with a precision in the order of 1μs.

The total height of the carrier must be recorded, as it provides the input parameter for the velocity calculation through the photoelectric switches. The switches used in the prototype are the Panasonic EX-11A-PN, which have been chosen due to the high repeatability (0.05mm), fast response time ($< 500\mu$s), narrow beam (1mm), as well as the robust construction against contamination and vibration. The same sensor is reading the arrival and leaving of the carrier on the beam, therefore both measurements have the same relative delay between each other, mitigating the error deriving by its response time.

3.3. Frame

The frame is composed of 20 $\times$ 20mm beams from the OpenBuilds®framework. Connections are made with 90° links. M5 T-nuts provide anchor points for the other elements.

A V-Groove gantry has been used to allow vertical movement of the slider, which is then locked in place by a screw and T-nut. Two T-nuts fixed in position at the top and bottom are the end-stops.

Four feet on the base allow the leveling of the device. The reference level for the whole system is placed by the electromagnet on the slider. A second level is used for the alignment of the anvil.

3.4. Microcontroller

Since both the accelerometer and photoelectric switch operate at 24V, and to improve the resilience of the apparatus, the choice fell to an industrial shield based on Arduino: the Sferalabs IONO MKR. The microcontroller integrates wireless connectivity capability through the WiFiNINA library. BLE connection was chosen because of it ease of direct connection with smartphone devices, and the data transfer rate is more than adequate. Communication is handled through a BLE UART

Fig. 4. Examples of sample stubs as-manufactured, prior to surface polishing. From the left, the materials are AISI 316L steel, PTFE, unalloyed copper (99.9%).

communication protocol, which is implemented through the HardwareBLESerial library. Small modifications to the device code can make it compatible with the more traditional Arduino serial protocol through USB. The version with Arduino MKR WiFi 1010 has been chosen to have at least two interrupt capable connections. The microcontroller is located in the electronics box on the back of the machine, visible in Fig. 5.

The mechanical design is available to view and duplicate here.

Fig. 5. Electronics box of the device, view from the back.

4. Design files summary

Design filename	File type	Open source license	Location of the file
Mechanical assembly	CAD files	CC-BY 4.0	Onshape repository
Blueprints	PDF	CC-BY 4.0	https://doi.org/10.5281/zenodo.7448231
Firmware sketch	INO	CC-BY 4.0	https://doi.org/10.5281/zenodo.7448231 Github
Pictures	JPG	CC-BY 4.0	https://doi.org/10.5281/zenodo.7448231
Assembly	STEP and PARASOLID	CC-BY 4.0	https://doi.org/10.5281/zenodo.7448231
toPrint	STEP and STL	CC-BY 4.0	https://doi.org/10.5281/zenodo.7448231

The information on this project is publicly available in the Zenodo repository. It includes the relevant design information: the firmware, the complete Bill of Materials, the complete CAD assembly in the standard STEP format, and additional pictures of the completed device.

Mechanical assembly is the complete CAD design, realized in Onshape®. The complete design can be cloned or exported. The file structure is self-explicative: the design files are organized in subfolders according to their hierarchy as subassemblies.

Blueprints are the complete design files for the device's structure, derived from the CAD design.

Firmware sketch is the Arduino sketch to load on the microcontroller. It is provided as a GitHub project.

Pictures of the completed device.

Assembly additional design files in Step format.

5. Bill of materials summary

The complete Bill of Materials is available through the Zenodo repository, here. It includes the cost of all the parts to be purchased. It also includes a list of the parts to be manufactured independently, either through FDM 3D printing or machining. The cost for the latter is only approximated, since it strongly depends on a variety of factors. The items in the summary have been grouped to streamline the present article, therefore the designator and unit price have been omitted.

Designator	Component	Number	Cost per unit - currency	Total cost - currency	Source of materials	Material type
–	3D printed parts (PLA)	9	–	€7.80	–	polymer
–	laser cut parts	2	–	€3	–	polymer
–	machined parts	8	–	€570	weerg.com	metal, polymer
–	Electronics	22	–	€621	RS and Mouser	various
–	Frame structure	98	–	€144	OOznest and RS	metal

6. Build instructions

Frame assembly #100–000

The mechanical part of the construction process follows the provided blueprints. The final object to be built is designated by part number #000–000.

- Build the frame #110–000 and slider #120–000, referencing the design #100–000 for the hardware locations. On the back of the slider there are three T-nuts: two fixed at the extremities acting as endstops, one free in the center. On the frame, T-nuts are placed wherever other elements will be connected.
- Add the feet #100–003 to the frame.
- Attach the gantry #110–002 using two T-nuts and low profile M5 bolts.
- Attach the Knob M5 - Support #130–002 using a long 20 mm T-nut and two low profile M5 bolts.
- Insert the slider #120–000 through the gantry #110–002. Lock it in place by inserting the extremity of the Knob M5 #130–000 through the central T-nut in the slider.

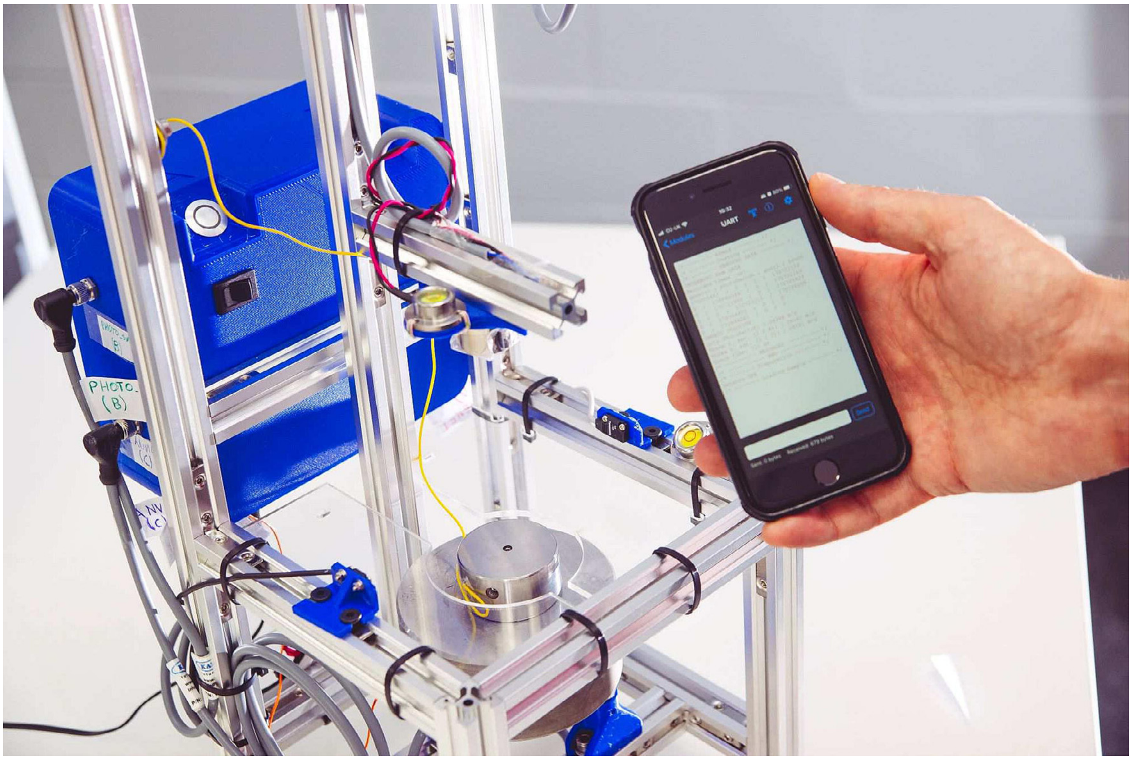

Fig. 6. The device communicates through BLE UART terminal emulation. Any smartphone can connect to the device by installing an open-source app.

Verify that the construction does not have excessive play, and that it does not warp when manipulated. Check the perpendicularity of the elements. Check the alignment of the slider with the frame. Check that the T-nuts have been positioned in the correct spots, which might not be accessible afterwards.

Anvil assembly #200–000

The anvil holds the accelerometer and switch on the bottom. They will be added at a later steps.

- Insert the spring sleeves in the corresponding slots of the anvil, according to the design #210–000. The sleeves can be fixed in place with some tape or a shim.
- Position the three Support brackets #220–001 on the frame. Loosely tighten the corresponding M5 bolts.
- Position the three adjustment screws #220–002, each with the corresponding M8 nut and spring according to the design #220–000.
- Position the anvil, and check the correct alignment of the supports #220–000. Tighten the M5 bolts to the structure.
- Level the anvil by acting on the M8 nuts, and check with one of the bullseye level.

Carrier #300–000

Insert the three M5 setscrews in the corresponding radial holes of #300–001. The Sample is inserted in the center. When using the sample's provided design and 90° point setscrews, it is effectively pushed against the bottom of the Carrier #300–001. If securely tightened, even stronger impacts are effectively transferred to the sample. If the sample side does not have a groove, slipping might occur.

If acquiring data using the contact information, add a soft cable to the carrier, which will be connected to DI6, according to the diagram provided in Fig. 7.

Accessories #400–000

- The circuit box #410–000 is mounted on the back of the device using four M5 bolts, attached to corresponding T nuts on the frame #100–000. Inside the box, the same two bolts used to attach it to the frame pass through the DIN rail, as visible from 5. The lid will be fixed in place by four low profile M5x12 bolts.
- The two element of the Photoelectric switch Panasonic EX-11A-PN are attached to the supports #420–002 using the provided M2 hardware. Each support is attached to the frame according to the assembly blueprint #000–000, using a 20mm long, 2xM5 T-nut. The cables are color coded as: Brown and Blue provide power, black signal. The black wire is present only on the receiver.

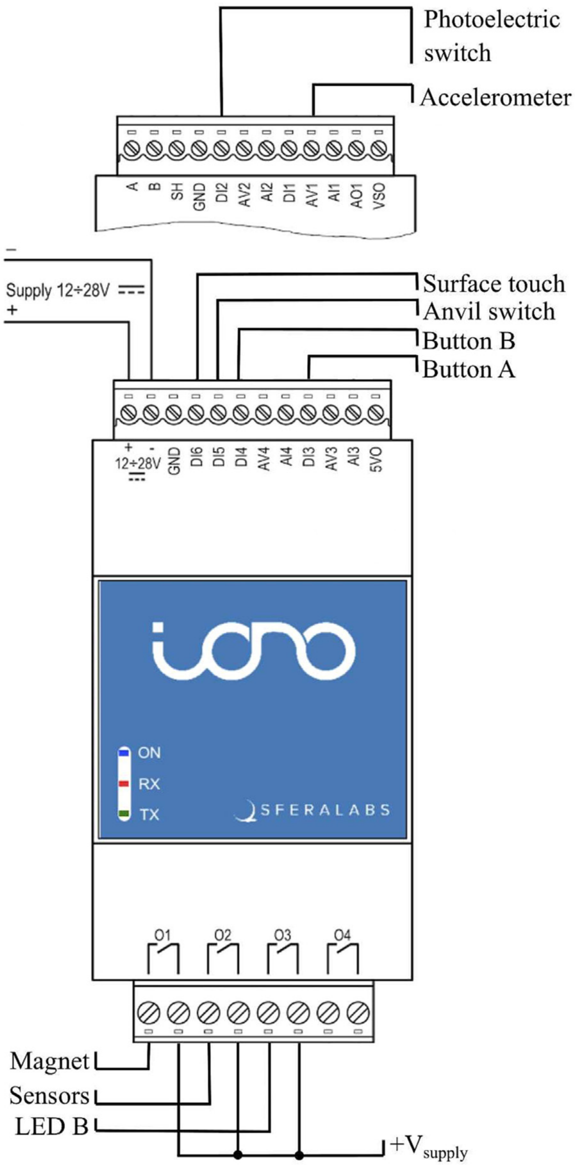

Fig. 7. Schematic of the connections to the iono MKR Microcontroller.

- The 25*mm* magnet is fixed in place on the support #430–003 using three countersunk M3x10 screws. The bullseye spirit level can be placed on the same support and fixed with either M2.5 hardware, double sided tape, or simply ties. The support assembly #430–000 is positioned on the slider and fixed with two T-nuts and corresponding M5 bolts.
- The shields, left and right, are fixed in place using six 3mm zip ties. It is suggested to leave this step as very last, as it blocks the anvil from sliding off in case the sensors on the bottom should be accessed.

Wiring The electronics box, visible in Fig. 5, contains the wiring between the microcontroller and the various elements of the device. The connections to the microcontroller are presented in the simplified diagram in Fig. 7.

The top of the box holds the two main control buttons, **A** and **B**, which in this case incorporate a status LED each. The LEDs are both connected to ground on one side. LED A is directly connected to **O1**, so it turns ON and OFF with the magnet. LED B is connected to **O3**. The buttons are connected to the positive supply voltage (VCC) and to the 24*V* tolerant inputs **DI3** and **DI4** of the IONO board. The inputs have an internal pulldown resistor path.

The power going to the sensors, i.e. the positive cables to photoelectric switch, accelerometer and vibration switch on the anvil, the anvil itself through a 10kΩ resistor, is switched ON only for the duration of the test by the relay contact indicated as **O2** in the simplified connection schematic in Fig. 7. The contact strips visible in Fig. 5 are, in order from left to right: the power to the sensors, GND, VCC. The power supply is connected to the bottom of the box using a standard 5.5mm barrel jack connection, and its positive side sees a rocker switch.

On the outside of the electronics box, the three industrial standard M8, 4 conductors, cables and connectors transport power and signal to the various parts of the device. The wire colors have been standardized as follows in the device:

- BROWN – Positive, VCC
- BLUE – Negative, GND
- WHITE – First signal
- BLACK – Second signal

Cable A goes to the slider. The blue wire is connected to the magnet's negative (black), and the white signal wire to the magnet positive, connecting it to **D1** on the diagram in Fig. 7. It is recommended to place a reverse biased diode between the magnet's terminals.

Cable B connects the middle section of the device. It brings power to the photoelectric switch elements, and the receiver's black wire is the signal. The brown wire is connected to the anvil through a $10\mathrm{k}\Omega$, 1/4W resistor. The white wire is connected to the carrier through a flexible extension wire, visible in yellow from Fig. 1.

Cable C connects the bottom of the anvil. The accelerometer is connected to the blue wire (GND) and to the white wire. Inside the Electronics box, a small prototyping board realizes the circuit shown in Fig. 3, and is connected to **AV1**. The vibration switch is connected to the positive brown wire and to the black signal wire, which leads to **DI5**.

7. Operation instructions

7.1. Sample preparation

The stub is the element providing the flat adhesion surface, the stub with particles on the surface is considered the sample. The stub can be either solid material or be the base for a thin substrate, for instance a glass slide or various coatings. The surface is cleaned and conditioned according to the desired specifications. The particles are then dispersed on the surface. The PSD and shape parameters before the test can be assessed using either scanning electron or optical microscopy. Knowing the PSD of the powder distributed on the sample and of the bulk can be useful to confirm the correct sampling. Image processing is carried on using Fiji [13] using segmentation techniques, which allows to process multiple images at the same time to obtain a statistically significant result. It is useful that the PSD is not too wide to aid in the image segmentation. It is also important to ensure the correct distribution of the particles on the substrate, avoiding overlap. Petean et.al. [14] use a Galai PD-10 powder disperser which minimizes the occurrence of agglomerates.

The substrate preparation is critical in the success of the experiment. It should provide the correct contrast with the powder, to aid with image segmentation, and not contain scratches or porosity which might be misinterpreted by the software. The user should pay close attention to surface roughness, as it has a huge influence on adhesion, and its effect is under active investigation [15]14. For metallic surfaces and particle size in the range of $20 - 100\mu$m, it is advisable to conduct a metallographic polish to obtain a surface whose roughness is not picked up by the optical microscope, and is smaller than the expected contact area. Fig. 8a shows how the presence of a deep scratch on the surface invalidates the measurement by providing a preferential location for particles to adhere.

Oxidation and surface contamination greatly affect surface adhesion, and the user must pay close attention. This device is presented as a meso-scale test, as opposed to AFM which is able to capture portions of a particle's surface. By employing the correct contact model, the user might select a surface treatment to represent the process conditions of interest. In the pre-

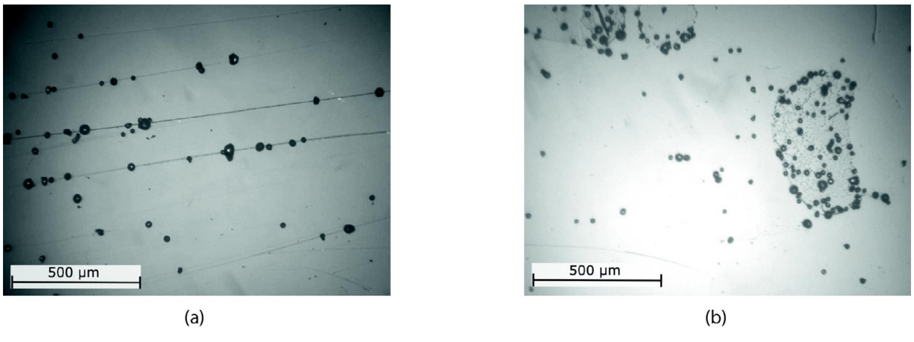

Fig. 8. Problematic areas after a test: (a) scratches provide a location of preferential adhesion; (b) residual oils or waxes after cleaning augment particle adhesion through liquid bridging. The particles are AISI 316L steel and the substrate is borosilicate glass.

sent iteration, surfaces have been lightly rubbed with acetone and left to evaporate under atmospheric conditions, before dispersing the powder to be tested. An example of liquid or wax contamination is presented in Fig. 8b, where the contaminant increases the particles' adhesion.

7.2. Test

Connection
The present discussion is for a BLE capable apparatus, based on the Arduino MKR wifi 1010.

- Turn on the apparatus from the main switch. The **B** button LED starts flashing slowly, waiting for a BLE connection.
- Open a BLE UART capable application on a smartphone (refer to the Arduino library HardwareBLESerial for a compatibility list). Once connection is established, the LED on the **B** button should have started flashing rapidly.
- When connected, enter the UART section of the application, then press the **B** button. The LED on the **B** button turns off, and information is transmitted through the BLE connection. The terminal should show the apparatus information and its activities.

The program sends instructions to the user through the UART terminal interface, reminding the steps to conduct the test, as they are described in the following points. A future implementation will use the same BLE library to send commands back to the device and update the configuration, which at this moment is done through variables declared in the first part of the sketch.

If the terminal is closed but the connection is active, the apparatus has no way of knowing. The data will be sent anyway and it might get lost. Before sending the test outcome, the apparatus checks the state of the connection. If the BLE connection is lost, the **B** LED starts flashing slowly, repeating the connection sequence just explained.

The output data displayed by the BLE UART terminal, see Fig. 6, can be either annotated or saved to a text file.

Preparation

- Adjust the drop height, using the dedicated knob, see Fig. 9b.
- Verify the alignment of the apparatus, using the bullseye level mounted near the magnet. If needed, adjust the four bottom feet.
- Verify the anvil alignment, placing a second bullseye level on top of it. If needed, correct the alignment using the three adjustment screws on the bottom.

Sample loading/unloading

- Carefully load the sample in the carrier, using the three setscrews to secure it in place, see Fig. 9a.
- Place the sample under the magnet, long press button **A** to activate the magnet, as in Fig. 9c. The magnet status is displayed by the LED on button A.
- If needed, long press **A** releases the sample, to correct the placement.
- Once the sample is retained by the magnet, long press button **B** to proceed to the next stage. Both LED **A** and **B** should be active.
- If needed, double press **B** can be used to revert to the loading phase.

Testing

- Long pressing buttons **A** and **B** simultaneously starts the test sequence see Fig. 9d. The apparatus' state is `armed`, the sensor power is turned on. During a timeout, the LED on button **B** is blinking.
- the operators should clear the machine, since the dropped sample might behave unpredictably on the rebound.
- If needed, a press of either button **A** or **B** during the timeout reverts to the loading phase.
- Once the timeout is over, the sample is dropped. The microcontroller records the event.
- The microcontroller checks the BLE connection and sends the test results.
- At this point the microcontroller goes back to the loading/unloading phase.

7.3. Sample evaluation

After the drop, the sample must be collected and carefully extracted from the carrier. Release the three setscrew; the hole in the back of the carrier can aid in the extraction. Using microscopic imaging, as discussed in Section 7.1, the resulting PSD is evaluated. If a microscope with an adequate focal length is available, the evaluation can happen with the sample still inserted in the carrier, reducing the risk of invalidating the test through mishandling.

The velocity measured by the machine, the recorded times, and optionally the acceleration, can be used to determine the adhesion parameter γ of the JKR contact model [2], or other contact models which the user might find more appropriate (for

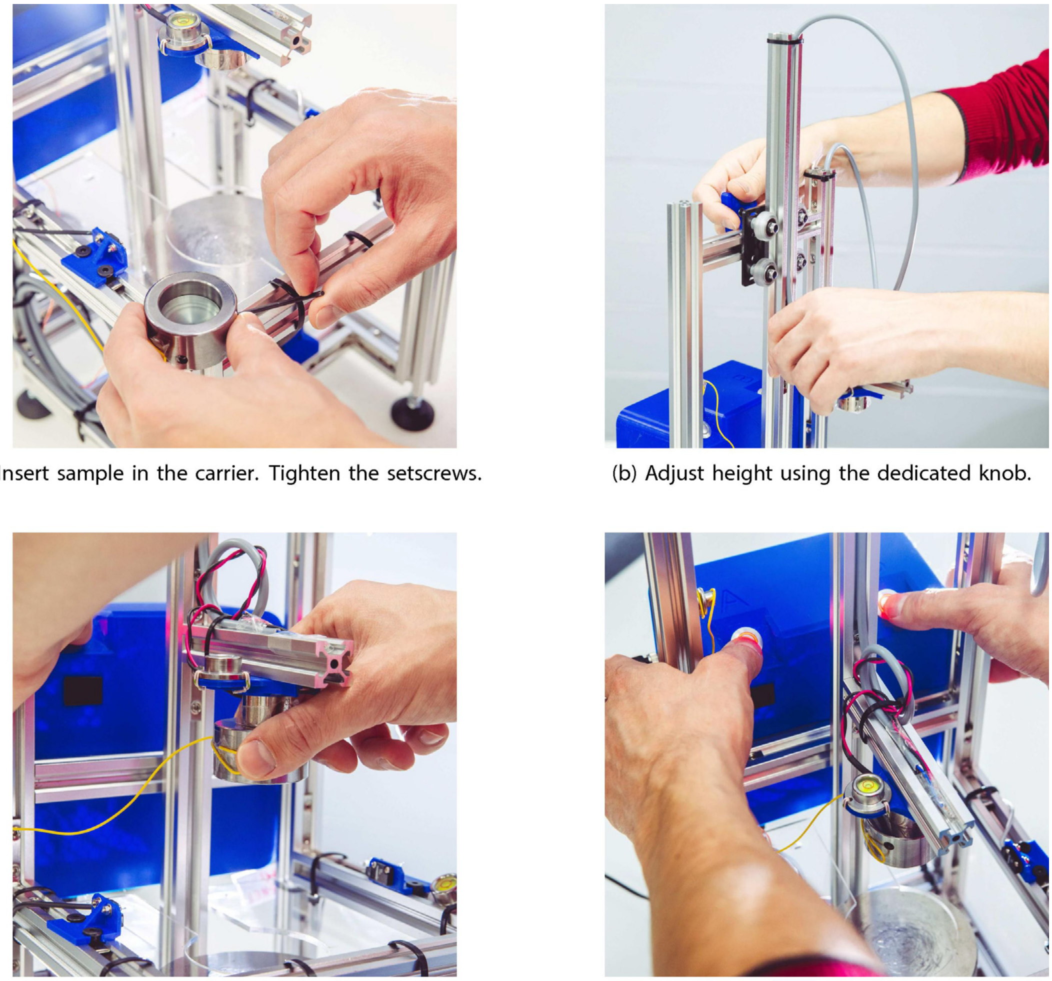

(a) Insert sample in the carrier. Tighten the setscrews.

(b) Adjust height using the dedicated knob.

(c) Press A to turn the magnet ON and hold the carrier.

(d) Press A & B to start the test sequence.

Fig. 9. Operation steps described in Section 7.

instance: Maugis-Dugdale, DMT). A useful tool to verify which model is more appropriate is the Tabor parameter [16]15, reported in Eq. 4. The JKR model can be considered exact for $\mu_T \gg 1$, but for very stiff cases the user might want to use either the DMT contact model ($\mu_T \ll 1$) or the Maugis-Dugdale model in intermediate cases. The user should also consider the necessity of taking into account the surface roughness [17].

$$\mu_T = \frac{h}{Z_0} = \left(\frac{R\Gamma^2}{E^{*2} Z_0^3}\right)^{\frac{1}{3}} \tag{4}$$

where R is the sphere rradius, Z_0 is the range of attraction of adhesive forces, close to atomic distance, and E^* is the reduced stiffness of the contact.

When using the JKR contact model, the procedure suggested by Zafar et al. [12] can be used to evaluate the critical diameter. The method involves measuring the adhesion force between particles and a glass surface and using image analysis techniques to determine the critical diameter, above which particles are detached and below which they remain attached for a given impact velocity. It assumes that a critical radius of the particles R_c can be determined, above which the detachment force is higher than the force of adhesion, resulting in Eq. 3. The authors used the Malvern Morphologi G3 instrument for pre-test and post-test image analyses of the sample to determine the projected area equivalent circle diameter (CE) of the particles. When considering more realistic rough surfaces, Petean et.al. [14] represent the adhesion force between the powdered material particles and the substrate surface by the geometric mean for adhesion force, which is defined as the force found after the centrifuge experiments, when there is a 50% probability that the particles remain adhered to the substrate surfaces. The authors used optical microscopy and a segmentation software ([13]) to determine the diameter of the particles present on the substrate.

7.4. Potential safety concerns

Based on the experience gained from using this device, we believe that any mode of operation poses a negligible or very low risk. However, it is important to note that the current design does not include a containment unit for the material being tested. As a result, the highest risk factor comes from the sample itself, and the operator must always refer to the material safety data sheet.

The electromagnet is only activated when energized, meaning that the carrier is securely held only when external power is supplied. If power is lost, the carrier may fall unexpectedly, which would invalidate the test. However, this poses no danger due to the limited fall height. The decision to design the device this way was influenced by part availability, but it could be improved by using a degaussing-type electromagnet that would hold the carrier even in the event of a power loss and require an electrical signal to release it.

The piezoelectric accelerometer requires the highest voltage and is designed to run at 24V, which is within the safe handling limits set by the European General Product Safety Directive (GPSD) 2001/95/EC. There is one exposed connection for the contact detection between the carrier and anvil, as explained in Section 3.2. The carrier is connected to the microcontroller by a lead at ground potential through a high impedance input circuit, therefore posing no risk. The anvil is connected to the positive supply voltage only during the test sequence, and disconnected the rest of the time. Although a 10kΩ resistor limits the short circuit current to 2.4mA, it could still be harmful to other sensitive electronics.

Given the nature of the proposed device, none of the circuit components have undergone electromagnetic compatibility assessment. The accelerometer leads, carrier lead, and especially the electromagnet could generate electromagnetic noise that might affect very sensitive electronics nearby.

8. Validation and characterization

The device provides ground to standardize the procedure of a kinetic adhesion test. The sample can be prepared externally of the apparatus, and quickly loaded in the carrier. Since it is recessed, the whole surface of the sample can be used to disperse powder, and makes it practical to polish it. Some tests have been conducted with different treatment zones of the sample surface, allowing for comparative testing.

The photoelectric switches response time of 500μs is the main uncertainty in the velocity measurement, therefore it can be used on its own to roughly estimate the error. The datasheet does not indicate which percentile this value refers to, but a reasonable estimate is 3σ of a lognormal distribution, resulting in the Probability Density Function represented in Fig. 10. From this estimate, the 10th and 90th percentiles are respectively 178μs and 330μs, indicated by vertical lines. As the carrier crosses the switch's laser beam, two consequent interrupts take place. Both of these happen with similar delays. A value that is greater than about 99% of the errors is: $\delta t = 152\mu$s.

The sensor side of the switch has a 1mm aperture, accounted by the code, and a repeatability perpendicular to the sensing axis of less than 0.05mm, therefore this is the second on the list of contributing factors to the measurement error, with a worst-case error of 0.1mm. The third point used for the velocity estimation is the touch signal between carrier and anvil that, with a much smaller uncertainty of 1μs, does not contribute significantly to the measurement error. The code uses the conventional value of 9.81m/s^2 for the gravitational acceleration, which could be corrected to account for the geographical variation. Combining both considerations, for the highest design velocity of 4m/s, the error on the measured velocity is:

$$E(4\text{m/s}) = \left(\frac{L - \delta L}{\frac{L-\delta L}{v} + \delta t} - v\right) \cdot v^{-1} = 0.0277 \times v \tag{5}$$

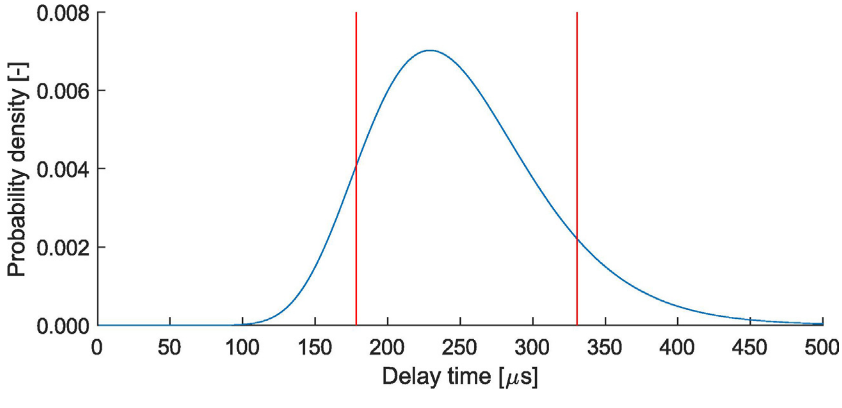

Fig. 10. Estimated lognormal distribution of the photoelectric switch's response time, assuming a 3σ specification of the response time from the manufacturer.

Plotting the theoretical error value against the effective velocity $v \leqslant 4\text{m/s}$, it approximates a line passing from the origin. For instance, the error at $v = 1\text{m/s}$ is $E(1\text{m/s}) = 0.0061 \times v$, or 0.61%. The contact time Δt registered by the microcontroller has been verified using a Tektronix 100MHz oscilloscope. The interrupt signals are registered within a few clock cycles, which happen at 48MHz for the selected device. This results in a rounding error smaller than $1\mu s$, since that is the unit used to report the total contact time, which is in the order of hundreds of microseconds.

The carrier has been dropped several subsequent times, for an expected velocity of around 1.2m/s, recording the measured values. This resulted in a standard deviation of around 1%. The accuracy of the device has been checked against the expected velocity determined by the sole drop height. Not accounting for the limited length measurement error, the measured data fall on average within 1.5% of the expected measurement, which is compatible with the previous considerations. The values are reported in Fig. 11.

Overall, the features of the proposed device are:

- Simple and guided impact test.
- Highly repeatable impact velocity and contact time measurement.
- Velocity estimation within $0.027 \times v$.
- Contact time recording within $1\mu s$.

8.1. Demonstration

The result of the test can be seen from Fig. 12. By analyzing the PSD before and after the test, it is possible to determine the diameter for which the adhesive energy balances the kinetic energy of the impact. A set of 10 images taken before and after the test were analyzed using the open-source suite Fiji [13], using segmentation techniques and obtaining a set of prop-

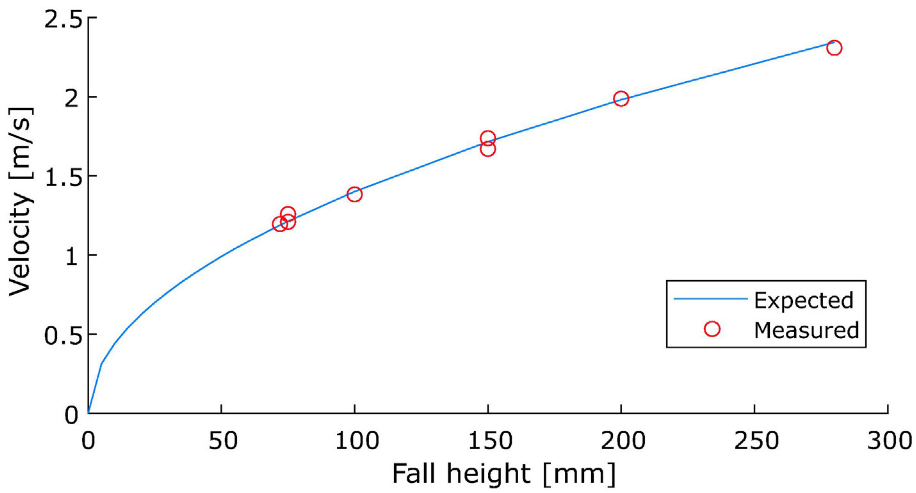

Fig. 11. Diagram of the measured velocity of the carrier compared to the expected values for an object falling from the same height under the action of gravity.

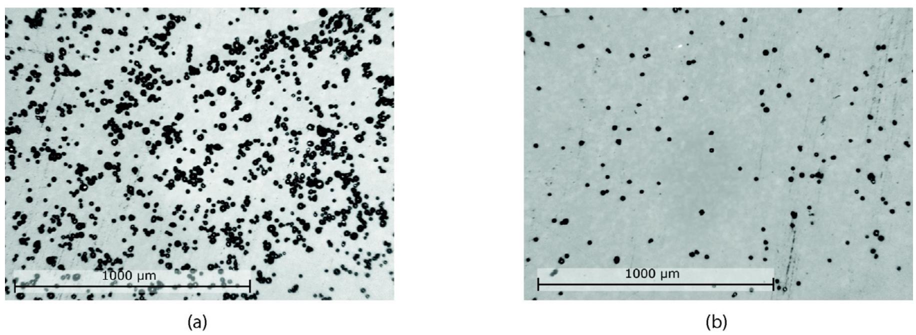

Fig. 12. Test results examples for 316L stainless steel powder dispersed on a borosilicate glass substrate, (a) before and (b) after the impact.

erties for each particle. For each particle the area resulting from the optical projection and binarized by the software, has been used to determine the equivalent diameter.

According to the formula proposed by Zafar et.al. [12], the critical diameter is estimated by finding the average diameter of the largest particle still attached to the surface and the smallest one detached. This is the procedure used in the presented examples. However, Petean et.al. [14] represent the adhesion force between the powdered material particles and the substrate surface by the geometric mean for adhesion force, which is defined as the force found after the centrifuge experiments, when there is a 50% probability that the particles remain adhered to the substrate surfaces. The user should select the most appropriate procedure according to their needs and the selected contact model.

This example analyzes an AISI 316L stainless steel powder, with a median grain size of $d_{50} = 35\mu$m and $d_{90} = 81\mu$m. The substrate is a borosilicate glass slide, securely glued to a stub using cyanoacrilate glue. The surface was cleaned with acetone and dry wiped.

The metal particles have a density of 7980kg/m^3, Young modulus $E_p = 2.11e11$Pa and Poisson ratio $\nu_p = 0.3$ [1]. The manufacturer's datasheet of the glass substrate reports $E_s = 6.4e10$Pa and $\nu_s = 0.2$. This gives the reduced stiffness $E^* = 5.5e10$Pa. The test has been conducted under atmospheric conditions.

In this case, the critical diameter was estimated to be $d_c = 45\mu$m, for a recorded impact velocity of 1.195m/s and a contact time between the impact surfaces of 102μs. With these values and the formula reported in Eq. 3 derived from the JKR contact model, the surface energy per unit area is $\Gamma = 0.168$J/m^2.

Assuming an interaction distance of $Z_0 \approx 0.3$nm [16], the Tabor parameter evaluated using Eq. 4 is $\mu_T = 2.06$, therefore the JKR contact model can be considered appropriate.

8.2. Limitations and future development

This device was designed to work in the same environment as the operator and the electronics, therefore at room temperature, humidity, pressure, and atmospheric composition. It is desirable to evaluate the influence of all these variables on the powder's cohesive properties. For example in additive manufacturing using the LMD process, the powders are subjected to temperatures that can be a significant fraction of the melting temperature, and very dry, inert transport gases. It is easy to imagine that the cohesive properties would change dramatically. The device could be made more compact by using a spring-loaded system instead of relying on gravitational potential energy. By enclosing the anvil and carrier in a containment tube, the atmospheric properties can be changed locally. A redesign of the carrier might provide the ability to contain the detached portion of the sample, reducing the contamination risk outlined in Section 7.4.

The minimum practical height from which the carrier can be dropped determines a minimum impact velocity of about 1m/s. Some material combinations or excessively large particle size might determine adhesion energies that are too small to balance the kinetic energy acquired at the indicated velocity. The general indication is that coarser powders can be characterized only for higher adhesive energy values. The opposite is also true: very fine powders might not be able to detach due to their lower inertia. This apparatus has been tested for steel and glass powders with particle sizes between 10 and 100μm, resulting in critical diameters between 25 and 60μm. Some measurements of stainless steel powder ($d_{10} = 21\mu$m, $d_{90} = 54\mu$m) on a very smooth and clean carbon steel substrate resulted in the total removal of the sample at the slowest impact velocity, invalidating the test. Further development could lower this limit, by changing the driving method to an active actuation or simply changing the position of the photoelectric switches.

Ethics statements

This work does not have any outstanding ethical implications.

CRediT authorship contribution statement

Lorenzo Pedrolli: Conceptualization, Methodology, Software, Data curation, Visualization, Writing – original draft. **Sadegh Nadimi:** Conceptualization, Methodology, Supervision, Resources, Funding acquisition, Writing – review & editing. **Sadaf Maramizonouz:** Conceptualization, Writing – review & editing. **Beatriz Achiaga Menor:** Supervision, Funding acquisition, Writing – review & editing. **Alejandro López:** Supervision, Writing – review & editing.

Declaration of Competing Interest

The authors declare that they have no known competing financial interests or personal relationships that could have appeared to influence the work reported in this paper.

Acknowledgements

This project has received funding from the European Union's Horizon 2020 research and innovation programme under the Marie Skłodowska-Curie grant agreement No. 847624. In addition, a number of institutions back and co-finance this project. The authors would like to acknowledge the contribution of the Engineering and Physical Sciences Research Council, EPSRC reference EP/V053655/1.

References

[1] W. Nan, M. Pasha, T. Bonakdar, A. Lopez, U. Zafar, S. Nadimi, M. Ghadiri, Jamming during particle spreading in additive manufacturing, Powder Technol. 338 (Oct 2018) 253–262.
[2] K. Johnson, K.K. A, and D. Roberts, Surface energy and the contact of elastic solids, Proc. R. Soc. London. A. Math. Phys. Sci., vol. 324, no. 1558, pp. 301–313, sep 1971.
[3] K. Johnson, H. Pollock, The role of adhesion in the impact of elastic spheres, J. Adhes. Sci. Technol. 8 (11) (Jan 1994) 1323–1332.
[4] H. Hertz, Ueber die berührung fester elastischer körper. J. die reine und angewandte Mathematik, vol. 92, pp. 156–171, 1882. [Online]. Available: https://eudml.org/doc/148490.
[5] D.M. Schaefer, M. Carpenter, B. Gady, R. Reifenberger, L.P. DeMejo, D.S. Rimai, Surface roughness and its influence on particle adhesion using atomic force techniques, Fundamentals of Adhesion and Interfaces, De Gruyter (Dec 1995) 35–48.
[6] N. Shukla, K.H. Henthorn, Effect of relative particle size on large particle detachment from a microchannel, Microfluid. Nanofluid. 6 (4) (Jul 2008) 521–527.
[7] Y. Hoshino, N. Kutsuwada, Y. Watanabe, H. Izawa, Measurement of van der waals force of toner adhesion employing a linearly increasing electric field and determining the toner jumping voltage, Part. Sci. Technol. 14 (3) (Jul 1996) 267–277.
[8] M. Ghadiri, M. Pasha, W. Nan, C. Hare, V. Vivacqua, U. Zafar, S. Nezamabadi, A. Lopez, M. Pasha, S. Nadimi, Cohesive powder flow: Trends and challenges in characterisation and analysis, KONA Powder Particle J. 37 (Jan 2020) 3–18.
[9] G.R. Salazar-Banda, M.A. Felicetti, J.A.S. Gonçalves, J.R. Coury, and M.L. Aguiar, Determination of the adhesion force between particles and a flat surface, using the centrifuge technique, Powder Technol., vol. 173, no. 2, pp. 107–117, Apr. 2007. [Online]. Available:https://www.sciencedirect.com/science/article/pii/S0032591006005493.
[10] Y. Shimada, M. Tsubota, and S. Matsusaka, Measurement of particle adhesion force and effective contact radius via centrifuge equipped with horizontal and vertical substrates, Powder Technology, vol. 397, p. 117103, Jan. 2022. [Online]. Available:https://www.sciencedirect.com/science/article/pii/S0032591021011219.
[11] K. Kendall, Cracks at adhesive interfaces, J. Adhes. Sci. Technol. 8 (11) (Jan 1994) 1271–1284.
[12] U. Zafar, C. Hare, A. Hassanpour, and M. Ghadiri, Drop test: A new method to measure the particle adhesion force, Powder Technol., vol. 264, pp. 236–241, sep 2014.
[13] J. Schindelin, I. Arganda-Carreras, E. Frise, V. Kaynig, M. Longair, T. Pietzsch, S. Preibisch, C. Rueden, S. Saalfeld, B. Schmid, J.-Y. Tinevez, D.J. White, V. Hartenstein, K. Eliceiri, P. Tomancak, and A. Cardona, Fiji: an open-source platform for biological-image analysis, Nature Methods, vol. 9, no. 7, pp. 676–682, Jul. 2012. [Online]. Available:https://www.nature.com/articles/nmeth.2019.
[14] P.G.C. Petean and M.L. Aguiar, Determining the adhesion force between particles and rough surfaces, Powder Technology, vol. 274, pp. 67–76, Apr. 2015. [Online]. Available:https://www.sciencedirect.com/science/article/pii/S0032591014010298.
[15] M. Ciavarella, J. Joe, A. Papangelo, and J.R. Barber, The role of adhesion in contact mechanics, Journal of The Royal Society Interface, vol. 16, no. 151, p. 20180738, Feb. 2019. [Online]. Available:https://royalsocietypublishing.org/doi/10.1098/rsif.2018.0738.
[16] D. Tabor, Surface forces and surface interactions, in Plenary and Invited Lectures, M. Kerker, A.C. Zettlemoyer, and R.L. Rowell, Eds. Elsevier, Jan. 1977, pp. 3–14. [Online]. Available:https://www.sciencedirect.com/science/article/pii/B9780124045019500092.
[17] B.N.J. Persson and M. Scaraggi, Theory of adhesion: Role of surface roughness, J. Chem. Phys., vol. 141, no. 12, p. 124701, sep 2014.

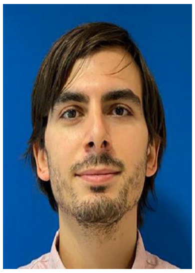

Mr Lorenzo Pedrolli (BSc, MSc) is enrolled in the PhD program in Engineering for the Information Society and Sustainable Development at the University of Deusto. He is part of the COFUND project 6i-DIRS, part of the Marie Sklodowska-Curie actions, under the Horizon2020 program. His research focuses on the modelling and simulation of the powder flow characteristics in additive manufacturing technologies. He received his BSc in Industrial Engineering and MSc in Mechatronic engineering at the University of Trento. This work has been developed during a mobility period at Newcastle University.

Dr Sadegh Nadimi (PhD FHEA MInstP) is an Associate Professor (Senior Lecturer) in the School of Engineering at Newcastle University. He holds a PhD in Geotechnical Engineering from City, University of London and MSc in Geotechnical Engineering from Newcastle University. Following the award of his doctorate, Sadegh moved to the University of Leeds as Post-doctoral Research Fellow studying tribology of particulate solids. Sadegh is committed to advancing fundamental engineering research and teaching. He is an Associate Editor of 'Géotechnique' and acts as a member of Editorial Board of 'Soils and Foundations', and 'Particuology'. He serves as Committee member on the Institute of Physics (IOP) Applied Mechanics Group.

Dr Sadaf Maramizonouz (BSc, MSc, PhD) currently works as a Post-doctoral Research Associate at Newcastle University. Her research interests include fluid mechanics, computational fluid dynamics (CFD), fluid-particle interactions, and discrete element method (DEM). She has received her BSc and MSc degrees in Aerospace Engineering from Sharif University of Technology and holds an PhD in Mechanical Engineering from Northumbria University Newcastle.

Dr Alejandro Lopez is a Lecturer in Applied Mechanics at the University of Deusto (Bilbao, Spain). His research focuses on CFD and DEM modelling of multiphase flows, erosion processes, cohesive powder flow and manufacturing processes, He worked as a Manager in the service industry in Spain before deciding to pursue an academic career. He received his PhD in Mechanical and Aerospace Engineering from the University of Strathclyde (Glasgow, UK), specifically studying erosion processes with CFD. After his PhD he joined Ghadiri Research Group (http://ghadiri-group.leeds.ac.uk/) before being recruited for his current position.

Dr Beatriz Achiaga is a Lecturer/Assistant Professor in the School of Engineering at Deusto University. She graduated with a PhD from Antonio de Nebrija University and a Master's Degree in Advanced Manufacturing. In recent years she has continued her research activity in the experimental and theoretical study of the mechanical characteristics of advanced powder materials such as silicon carbide, low-alloy and stainless steels. In addition, she has participated in various projects with companies and has extensive experience in manufacturing through advanced industrial processes of metallic, ceramic and polymeric components.